Impervious Surface Extraction From Multispectral Images via Morphological Attribute Profiles Based on Spectral Analysis

Changyu Zhu, Jun Li, *Senior Member, IEEE*, Shaoquan Zhang, Changshan Wu, Bing Zhang, *Senior Member, IEEE*, Lianru Gao, *Senior Member, IEEE*, and Antonio Plaza, *Fellow, IEEE*

***Abstract*—Impervious surfaces exhibit unique spatial characteristics in urban environments. The estimation of impervious surfaces is critical for the analysis of these environments. In this paper, we propose a new technique based on morphological attribute profiles for mapping impervious surfaces under a spectral mixture analysis model. A main feature of our newly developed method is that it can model different kinds of structural information, which represents an important competitive advantage over existing techniques. As a result, considering the special characteristics of urban environments, our new method for impervious surface extraction exhibits the potential to model complex urban backgrounds. Four kinds of remotely sensed data, including Landsat ETM+, GF-1, IKONOS and sentinel-2 collected over Guangzhou, China, are used in this work to test the performance of our approach in the task of extracting imperviousness from images with different spatial resolution. Our experimental results illustrate that the proposed method exhibits very good performance in the task of estimating the impervious surface distribution, with relatively high precision. Root-mean-square error (RMSE) was 10.89%, mean absolute error (MAE) was 8.37% and Bias was 1.4% for the ETM+ data. RMSE was 11.49%, MAE was 6.25% and Bias was 2.34% for the GF-1 data. The RMSE was 7.72%, MAE was 7.67% and Bias was 3.91% for the IKONOS data, respectively. These results are superior to those provided by other state-of-the-art methods. Furthermore, our results also show the effectiveness of the method in distinguishing bright impervious surface from the dark impervious surface, especially in high resolution remotely sensed images.**

***Index Terms*—Impervious surface, morphological attribute profiles (MAPs), multispectral images, spectral mixture analysis (SMA).**

Manuscript received February 3, 2018; revised April 26, 2018 and July 3, 2018; accepted July 5, 2018. Date of publication November 28, 2018; date of current version December 31, 2018. The work of C. Zhu was supported in part by the National Natural Science Foundation of China under Grant 61771496, in part by the National Key Research and Development Program of China under Grant 2017YFB0502900, and in part by the Guangdong Provincial Natural Science Foundation under Grant 2016A030313254. *(Corresponding author: Jun Li.)*

C. Zhu is with the Guangdong Provincial Key Laboratory of Urbanization and Geo-Simulation, School of Geography and Planning, Sun Yat-sen University, Guangzhou 510275, China (e-mail: zhuchy8@mail2.sysu.edu.cn).

J. Li is with the College of Electrical and Information Engineering, Hunan University, Changsha 410082, China (e-mail: lijun8206@hnu.edu.cn).

S. Zhang is with the Jiangxi Province Key Laboratory of Water Information Cooperative Sensing and Intelligent Processing, Department of Information Engineering, Nanchang Institute of Technology, Nanchang 330099, China (e-mail: zhangshaoquan1@163.com).

C. Wu is with the tDepartment of Geography, University of Wisconsin-Milwaukee, Milwaukee, WI 53201 USA (e-mail: cswu@uwm.edu).

B. Zhang and L. Gao are with the Key Laboratory of Digital Earth Science, Institute of Remote Sensing and Digital Earth, Chinese Academy of Sciences, Beijing 100094, China (e-mail: zb@radi.ac.cn; gaolr@radi.ac.cn).

A. Plaza is with the Hyperspectral Computing Laboratory, Department of Technology of Computers and Communications, Escuela Politécnica, University of Extremadura, E-10071 Cáceres, Spain (e-mail: aplaza@unex.es).

Color versions of one or more of the figures in this paper are available online at http://ieeexplore.ieee.org.

Digital Object Identifier 10.1109/JSTARS.2018.2877768

I. Introduction

IMPERVIOUS surfaces, defined as any surface that water cannot infiltrate, are associated with transportation features (e.g., streets, highways, parking lots, and sidewalks) and building rooftops [1]–[3]. With the development of urbanization in the past 30 years, natural and agricultural land cover has been lost due to aggressive expansion of impervious surfaces. The increase of impervious land covers is expected to result in an increase in the volume, duration, and intensity of urban runoff [4]. Moreover, imperviousness can also affect the nonpoint source pollution and water quality of surrounding lakes and streams [5]. Therefore, impervious surfaces can provide a measure of the environmental quality and level of urbanization of a city. It is therefore important to estimate the extent of impervious surfaces for regional water environment planning, land use planning, urban ecological research, urban land use change monitoring, population estimation, etc. [6], [7].

Remote sensing has been an important and effective technology for the estimation of impervious surfaces. With a synoptic view and frequent revisits over large areas, numerous methods exploiting the spectral, spatial, and contextual information contained in remotely sensed datasets have been developed for urban environment analysis [8]. Ridd [9] proposed a new urban environmental components model, in which urban surfaces are expressed as the combination of three different elements, i.e., vegetation, impervious surfaces, and soil (V-I-S). This model provides a theoretical basis for analyzing the urban landscape from remote sensing imagery, in which it is assumed that a pixel is generally a mixture of vegetation, impervious surface, and soil in certain proportions. However, the V-I-S model is only considered conceptually, with limited applications because of the difficulties involved in the estimation of impervious surfaces [8], [10]. Hence, many applications have been developed to handle this problem under the assumptions of a V-I-S model. Spectral mixture analysis (SMA), aimed at analyzing the fractions of each spectral component (known as *endmembers*), is an effective method to estimate impervious surfaces, as indicated by

several works that focused on this research direction [11], [12]. For instance, Wu and Murray [10] proposed a four-endmember model, including vegetation, soil, high albedo, and low albedo, to estimate impervious surfaces by using multiple remote sensing images. Sun *et al.* [13] presented a stratified SMA in spectral domain (Sp_SSMA) for impervious surface mapping, indicating that the Sp_SSMA method achieves a better performance than full-set-endmember SMA and prior-knowledge-based spectral mixture. Powell *et al.* [14] mapped the urban land cover surface in subpixel scale with ETM+ imagery by using the multiple endmember SMA (MESMA) approach. Tang and Xu [15] used hyperspectral remote sensing images to extract the impervious surface via SMA model.

SMA-based methods have obtained very promising results in the task of characterizing impervious surfaces. However, these methods still face a critical issue that remains unsolved. That is, how to select/generate the pure spectral signatures of the considered endmembers [16]–[19]. There are many spectral unmixing algorithms which can be used for endmember extraction purposes, such as N-FINDR [20], orthogonal subspace projection [21], vertex component analysis (VCA) [22], and manifold regularized nonnegative matrix factorization [23], which obtained good performance in hyperspectral unmixing. However, most of them were originally proposed for hyperspectral images and it is very difficult to directly adopt them in multispectral image analysis, mainly due to the following reasons. On the one hand, the number of bands in multispectral images is smaller, which results in ill-posed unmixing problems [24]. On the other hand, there is a strong spectral variability in urban areas, which makes the unmixing problem even more difficult. For instance, constructions made up of the same materials may exhibit different reflectance properties [25], and different kinds of vegetation may exhibit strong spectral similarity [26]. Owing to the fact that it is very difficult to increase the number of spectral features in multispectral images, most works focused on tackling the aforementioned problems by addressing the issue of spectral variability. Especially, MESMA [14] is an effective method to address this issue. Furthermore, Li and Wu [27] introduced a geostatistical temporal mixture analysis approach to solve for the endmember variability for estimating regional impervious surface distributions.

By relaxing the importance of the endmember extraction step, the aforementioned methods (especially MESMA) have achieved very promising performance in the characterization of impervious surfaces [14], [28]. However, the selection of multiple spectral signatures still remains a challenging issue due to the small number bands present in multispectral data sets. There are several works that have focused on improving this aspect. For instance, Somers *et al.* [29] carefully select a certain wavelength (against the spectral variability) to generate robust endmembers. In turn, [30] and [31] transform the raw bands in the original image into a subspace to select the most representative endmembers. Spectral weighting (e.g., assigning higher weights to the spectral bands that are less sensitive to endmember variation) has also been adopted to address this issue [32], [33].

In order to improve the estimation accuracy in the case in which a small number of spectral signatures per endmember is used (i.e., one signature per endmember), it is important to address the representativeness of the selected spectral signatures, which becomes a critical aspect. Since most of the aforementioned methods focus on the characterization of the spectral information in the multispectral image, one possibility is to consider spatial information in addition to spectral information [34]. Based on Tobler's principle that *everything is related to everything else, but near things are more related than distant things* [35], we can assume that the same land cover entities with certain attributes are homogeneous, to some extent. As the spatial information of an object can describe its structure well, as well as its contextual and distribution characteristics, we propose to exploit this property to improve the endmember identification in multispectral images. In the literature, there are many works that take advantage of spatial information to extract the spectral signatures of the endmembers. Plaza *et al.* [36] proposed an automated morphological endmember extraction (AMEE) approach based on mathematical morphology to integrate the spatial and the spectral information in endmember extraction. Rogge *et al.* [37] proposed a spatial-spectral endmember extraction (SSEE) algorithm in which spatial constraints were utilized as a relevant criterion to separate different types of endmembers with similar spectral signatures. Both AMEE and SSEE were originally developed for hyperspectral images. Deng and Wu [38] proposed a spatially adaptive SMA (SASMA) technique to automatically extract and synthesize the endmembers for multispectral images. In [39], the paper offers robustness and flexibility in modeling scene images and reporting the improvements of the accuracy in scene recognition. The aforementioned methods nested the spatial information into the unmixing procedure through the use of a local search window. As urban environments are generally difficult to model, it is very challenging to define the size of the searching window in advance. It is known that artificial constructions (such as buildings) exhibit completely different spatial characteristics [40]. For example, a building (as an individual entity with small spatial scale) presents certain construction attributes, while a set of tightly arranged houses (covering a larger spatial scale) often present more regular contextual information. Another possible example is roads, which may exhibit different directional features. Therefore, new tools able to exploit and characterize spatial structures are needed to improve the extraction of impervious surfaces in urban environments.

Morphological attribute profiles (MAPs), proposed in [41], use four different structural attributes including area, length of bounding box, standard of deviation, and moment of inertia, to extract the spatial information in a hierarchical level via a tree graph model, providing a powerful tool for the characterization of spatial features in the image. Different from traditional morphological profiles, which extract the spatial information by using simple searching windows, MAPs can exploit more complicated structures and are effective for the interpretation of spatial information in remotely sensed images containing artificial, man-made objects [41], [42]. Specifically, the use of MAPs involves a process of feature space reconstruction, in which new feature spaces with certain spatial information are generated from raw images.

In this paper, we aim at exploiting the potential of MAPs for the extraction of impervious surfaces from multispectral

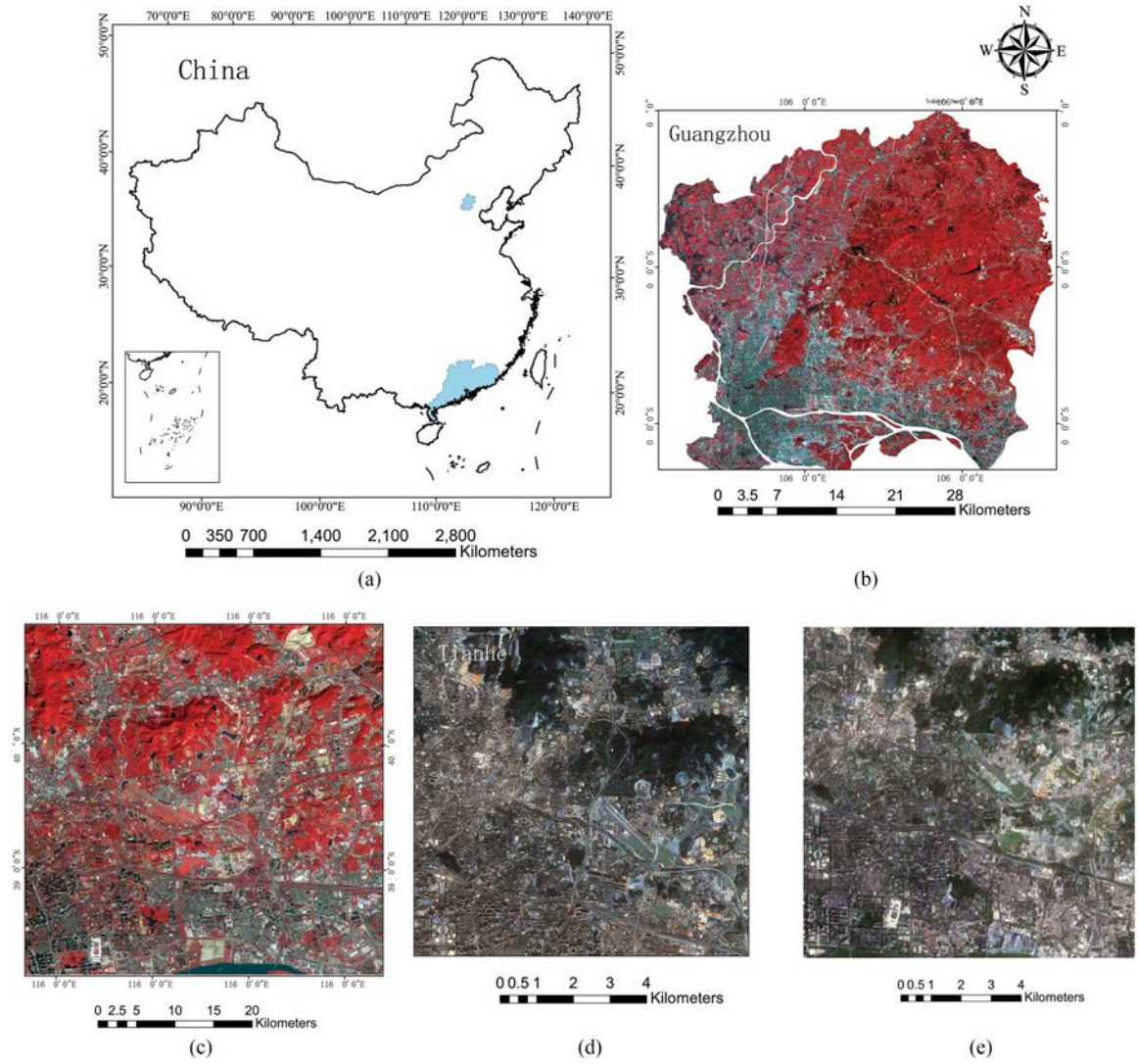

Fig. 1. Study areas and datasets. (a) Location of the considered areas in China. (b) False-color ETM+ image of Guangzhou. (c) False-color GF-1 image of Tianhe district in Guangzhou. (d) True-color IKONOS image of the Tianhe district in Guangzhou and (e) True-color Sentinel-2 image of the Tianhe district in Guangzhou.

images, with the ultimate goal to introduce a completely new framework (under the SMA model) for the characterization of imperviousness, supported by the spatial information extracted by MAPs. Since MAPs are highly effective at characterization of spatial details (which are more significant in medium-to-high spatial resolution images), four kinds of image data with different spatial resolutions, i.e., Landsat ETM+, GF-1, IKONOS, and Sentinel-2, are considered in this research. This is consistent with the fact that impervious surfaces (and other land covers) generally exhibit very different spatial structures under different resolutions.

The remainder of this paper is organized as follows. Section II introduces the study areas and the considered data sets. In Section III, we introduce the new methodology presented in this paper. The criteria used to conduct accuracy assessment are also indicated in Section III. Our experimental results are presented and discussed in Section IV. Finally, Section V concludes the paper with some remarks and hints at plausible future research lines.

II. Study Areas and Datasets

In this research, two different areas, the city of Guangzhou, China and the Tianhe district of Guangzhou (see Fig. 1), are chosen for analysis purposes. The total areas of the study sites are 719 and 141 km^2 for Guangzhou and the Tianhe District, respectively. These areas have experienced a fast development during the past 30 years, giving rise to significant urban development and a change of natural landscapes, in Guangzhou. The areas comprise many types of impervious land covers, such as parking lots, roads, and buildings. Additionally, there are also pervious surfaces in these areas, including grassland, tree/shrubs, cropland, and bare soil.

Four types of remotely sensed images (with different spectral and spatial resolutions) were selected for validation purposes, including 1) Landsat 7 ETM+ images with 6 bands and 30-m spatial resolution acquired on February 22, 2008 over Guangzhou, 2) GF-1 image with 4 bands and 8-m spatial resolution acquired on April 4, 2011 over Guangzhou, 3) IKONOS

image with 4 bands and 4-m spatial resolution acquired on February 1, 2009 over Guangzhou, and 4) Sentinel-2 image with 4 bands and 10-m spatial resolution acquired on July 7, 2017 over Guangzhou. These images were cloud-free. These images are converted to normalized exoatmospheric reflectance measures [43], [44]. Moreover, accuracy was assessed using two Quickbird images acquired in August 2008 over the city of Guangzhou, with resolution of 2.5 and 0.6 m for the multispectral and panchromatic images, respectively. Another QuickBird image acquired in October 2010 over Beijing is also used for validation. The reference data covered most of the study area, especially the regions that are full of impervious surfaces. All of these data are spatially aligned by geometrical correction [43], [45]. It should be noted that we assumed that there were no apparent changes in impervious surfaces among such images, due to their close acquisition time. By fusing the multispectral and panchromatic images via the fast Fourier transform (FFT) enhanced intensity, hue, saturation (IHS) transform method [46], we obtained multispectral images with 0.6-m resolution which are used for accuracy validation purposes. It should be noted that we chose the FFT-enhanced IHS transform method as it has been shown to be effective for the fusion of multispectral and panchromatic images [47]. In the validation, the ground reference data were obtained through manual digitalization, and each pixel in the QuickBird images is regarded as pure after color fusing and uniforming.

III. Methodology

In this section, we illustrate the performance of the newly proposed technique for the extraction of impervious surfaces, which includes three steps. First, new feature spaces containing spatial information were generated from the raw remote sensing data by using MAPs. Since the raw data itself contain spectral information, the newly obtained features explicitly integrate spatial and spectral information. After obtaining the new feature spaces by using MAPs, we perform VCA to automatically extract multiple endmember spectral signatures from the aforementioned feature spaces, along with their corresponding abundance maps. Finally, the impervious surface is estimated based on the unmixing results obtained from the SMA model.

A. MAPs

MAPs, as a new generation of morphological profiles (MPs) [41], are an extension of attribute profiles (APs) constructed via morphological operators by using different kinds of structuring elements. It should be noted that four attributes have been considered for the generation of the new features in this paper [42]. These attributes include the moment of inertia (which measures the elongation of the regions), standard deviation (which measures the homogeneity of the regions), length of diagonal of the bounding box (related to the folding degree of the regions), and area (related to the size of the regions). We use the aforementioned four attributes for two reasons. On the one hand, artificial objects present very different structures with different characteristics. For example, block buildings can be differentiated in the profiles constructed by using the area attribute. In turn, linear entities such as roads and streets can be distinguished by using moment of inertia attributes. On the other hand, these four different attribute profiles can comprehensively characterize complex urban structures, and at the same time reduce the collinearity among the feature spaces.

The filtering operation implemented in MAPs is based on the evaluation of how a given attribute $\mathcal{A}$ is computed for every connected component of a grayscale image f for a given reference value λ. For a connected component of the image C_i if the attribute meets a predefined condition [e.g., $\mathcal{A}(C_i) > \lambda$] the region is kept unaltered; otherwise, it is set to the grayscale value of the adjacent region with closer value, thereby merging C_i to a surrounding connected component. When the region is merged to the adjacent region of lower (or greater) gray level, the operation performed is called thinning (or thickening). Given an ordered sequence of thresholds $\{\lambda_1, \lambda_2, \ldots, \lambda_n\}$, an AP is obtained by applying a sequence of thinning and thickening operations, as follows:

$$\mathrm{AP}(f) = \{\phi_n(f), \ldots, \phi_1(f), \gamma_1(f), \ldots, \gamma_n(f)\} \quad (1)$$

where ϕ_i and γ_i, respectively, denote the thickening and thinning transformations [48]. Problem (1), which can be efficiently computed by applying a Max-tree algorithm [49], focuses on a single feature (or spectral band) of the image. For multispectral images, we can perform attribute filtering on the original data by treating each band separately. In other words, the MAPs can be obtained by generating APs on each of the bands of the multispectral data, thus building stacked features. Let $f = \{f_1, \ldots, f_b\}$ be a multispectral dataset with b bands. The following definition of the MAP can be considered:

$$\mathrm{MAP}(f) = \{\mathrm{AP}(f_1), \mathrm{AP}(f_2), \ldots, \mathrm{AP}(f_b)\}. \quad (2)$$

From the definition in (2), the consideration of multiple attributes leads to the concept of MAPs, which combines multiple APs by concatenating them as stacked features, and improves the capability of extracting the spatial characteristics of the structures in the scene.

B. SMA

Under the assumption of the SMA model, each pixel in the multispectral image is regarded as a mixed reflectance of different types of pure land covers (namely *endmembers*) with certain proportions (namely *abundances* or *endmember fractions*) [50]. The SMA model can be subclassified into linear and nonlinear, based on an assumption regarding the scattering (single or multiple, respectively) [32], [51]. It is known that multiple scattering can introduce significant nonlinear effects in the data [52]. However, in our context it can be assumed to be negligible due to the fact that second-order scattering is relatively weak in urban scenes [52]–[54]. Furthermore, our adoption of an MAP-based feature extraction strategy can greatly improve the linearity of the data [55]. Therefore, we only consider the linear spectral mixture model in this paper. This model can be simply defined as follows:

$$R_b = \sum_{i=1}^{p} f_i R_{i,b} + e_b \quad (3)$$

where R_b is the reflectance for the bth feature in the remotely sensed image, p is the number of endmembers, f_i is the fraction of endmember i, $R_{i,b}$ is the reflectance of endmember i in the bth feature, and e_b is the residual. Notice that if we perform SMA on the original image, b refers to a spectral band. In turn, if we perform SMA on the new feature space obtained after applying MAPs, b refers to a specific feature.

1) Automatic Endmember Extraction: Endmember extraction is the core procedure for the SMA-based estimation of impervious surfaces. Under the linear mixture model, the precision strongly depends on the quality of the extracted endmembers, as the abundance fractions of such endmembers will directly affect the accuracy of the estimation of impervious surfaces. Generally, there are two kinds of methods for endmember extraction, i.e., manual and automatic. Manual methods aim at selecting the pixels which minimize the within-class variation and maximize the between-class variation. This can be achieved by choosing the bands that exhibit high variation among different land covers, or by transforming the exoatmospheric reflectance bands into a subspace in order to select the most representative endmembers. On the other hand, automatic endmember extraction is a very active research topic as it can find the endmembers from the image data directly, without the need for manual intervention. There are many algorithms belonging to this category. Among those methods, we have selected the VCA [22], which has been shown to extract the endmembers with very good performance and low computational complexity. Herein, we assume that the VCA algorithm is used to extract the endmembers. Nevertheless, it should be noted that several other automatic methods can also be adopted for this purpose [24].

2) Estimation of the Abundance Fractions: Generally, it is assumed that the abundances are nonnegative and that the sum of abundances in each pixel equals to one, i.e., $\sum_{i=1}^{p} f_i = 1$, $f_i \geq 0$. The feasibility of these constraints has been discussed in many works [56]–[58]. Nevertheless, these two assumptions have been shown to be effective in real scenarios, as the reflectance in natural scenes generally follows them. Under these two assumptions, the abundances of different endmembers in a given pixel can be precisely estimated by the fully constrained least-squares linear method [58] as follows:

$$f_i = R_{i,b} R_b / \sum_{i=1}^{p} R_{i,b}^2. \tag{4}$$

C. Impervious Surface Calculation

In this paper, following [10]—in which it was concluded that the impervious surfaces are generally represented by low or high albedo endmembers—we use such low/high albedo endmembers to linearly represent the surfaces as follows:

$$R_{\text{imp},b} = f_{\text{low}} R_{\text{low},b} + f_{\text{high}} R_{\text{high},b} + e_b \tag{5}$$

where $R_{\text{imp},b}$ is the reflectance spectra of impervious surfaces for band b, $R_{\text{low},b}$ and $R_{\text{high},b}$ are the reflectance spectra of low albedo and high albedo for band b, f_{low} and f_{high} are the weights of low albedo and high albedo, respectively, under the assumption that $f_{\text{low}} + f_{\text{high}} = 1$ and $f_{\text{low}}, f_{\text{high}} \geq 0$, and e_b is the unmodeled residual. At this point it is worth noting that based on the SMA framework, each land cover can be represented by a unique endmember signature. Therefore, we can simply discriminate the high and low albedo based on the difference of their signatures.

Based on the fact that some land covers (such as water and shadow) are characterized by low albedo endmembers, it is difficult to directly apply (5) for the estimation of impervious surfaces. In order to improve the precision of the estimation of such surfaces, a preprocessing step is first performed in this paper for water-removal purposes. In particular, for the ETM+ images, the water regions are extracted and then masked out using normalized difference water index [59]. For the IKONOS images, water regions are extracted and then masked out using an unsupervised classification technique [10]. It should be noted that we are aware that the impact of shadows are significant in high-resolution images and shadow restoration is of great necessity prior to linear spectral unmixing because it is able to reduce spectral confusion between shadow areas and low albedo land covers in nonshadow areas [60]. Nevertheless, in this paper, the phenomenon of shadows are not considered as we empirically observed that the proposed approach can obtain very good performance without removing the shadow effects.

D. Accuracy Analysis

To evaluate the performance of the proposed method, three widely used error measurements, i.e., root-mean-square error (RMSE), mean absolute error (MAE), and Bias, were adopted [61], which are formally given as follows:

$$RMSE = \sqrt{\frac{1}{N} \sum\nolimits_{i=1}^{N} (imp_i - \widehat{imp_i})^2} \tag{6}$$

$$MAE = \frac{1}{N} \sum_{i=1}^{N} |imp_i - \widehat{imp_i}| \tag{7}$$

$$Bias = \frac{1}{N} \sum_{i=1}^{N} (imp_i - \widehat{imp_i}) \tag{8}$$

where imp_i is the impervious surface fraction of pixel i (as modeled by the proposed method), $\widehat{imp_i}$ is the actual impervious surface fraction of pixel i, obtained through human interpretation of the QuickBird images, and N is the total number of samples. Notice that both RMSE and MAE are able to quantify the abundance estimation error of different land covers modeled by the proposed method. Comparatively, as a measurement of bias, the Bias indicates an overall tendency regarding (upward or downward) estimation bias.

E. Comparison With Other Methods

To evaluate the performance of our newly proposed method for impervious surface estimation, we consider two method for comparison purposes.

1) Traditional SMA Framework: The traditional SMA framework applied to the raw bands of the original data are considered for comparison purposes [10]. Specifically, the raw bands of the original image are first transformed into new subspaces by using the maximum noise fraction (MNF)

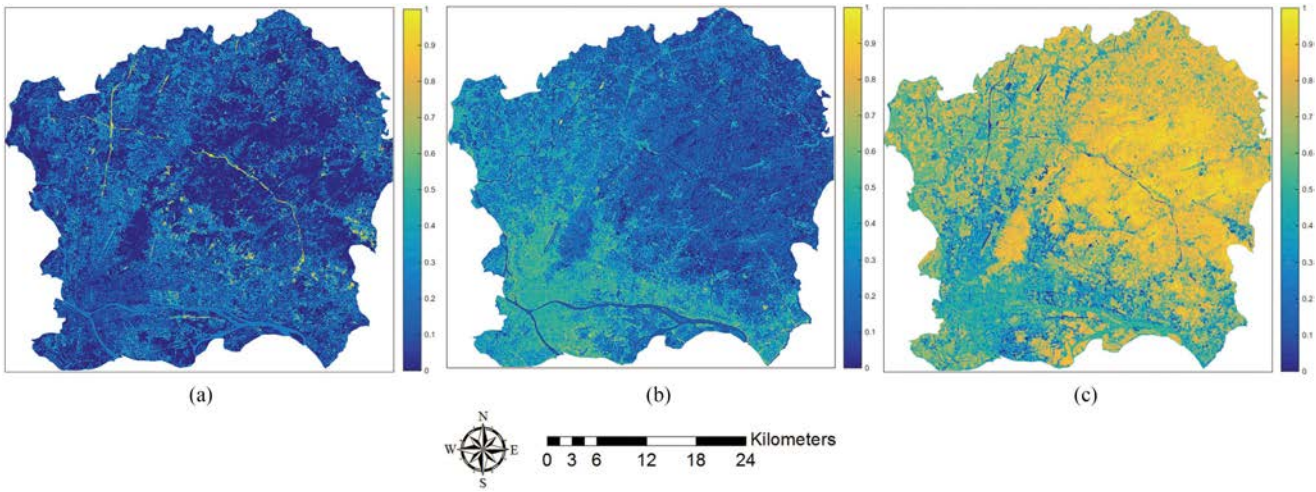

Fig. 2. Three fraction images obtained from the ETM+ image (Guangzhou). (a) Low albedo. (b) High albedo. (c) Vegetation.

TABLE I
IMPERVIOUS SURFACE ESTIMATION ACCURACY OF THE PROPOSED METHOD (ETM+ IMAGES)

Images	Methods	Areas	RMSE(%)	MAE(%)	Bias(%)
ETM+	Proposed	Developed area (imp$\geq$ 30%)	10.82	8.29	-5.07
		Less developed area (imp$<$ 30%)	11.04	8.45	7.9
		Overall	10.89	8.37	1.40
	Raw bands [10]	Developed area (imp$\geq$ 30%)	11.49	12.47	-10.26
		Less developed area (imp$<$ 30%)	10.01	12.56	9.04
		Overall	12.33	12.26	-5.96
	BCI [63]	Developed area (imp$\geq$ 30%)	11.71	19.67	-12.77
		Less developed area(imp$<$ 30%)	12.15	13.19	10.86
		Overall	12.21	16.43	-4.82

transformation [62]. Then, the endmembers are selected from the first three MNF components, where the most representative endmembers are located at the corners of the transformed feature space. Finally, the fractions of each endmember and the impervious surfaces are extracted by the SMA model.

2) Biophysical Component Index (BCI): To examine the performance of the proposed method, BCI was used for comparison [63], where BCI has been shown to be linear and positively correlated with the impervious surface.

BCI is first derived by a Tessel-Cap (TC) transformation from raw remote sensing images. We refer to [64] and [65] for more information about the TC transformation of TM and IKONOS images. Furthermore, BCI is calculated by using the first three components of the TC-transformed space. It is worth noting that to the best of our knowledge there is no research applying TC transformation to GF-1 images. Therefore, no experimental comparison with BCI is considered for the GF-1 case.

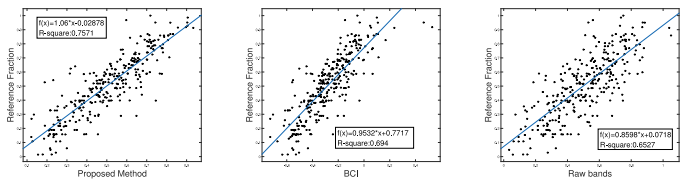

Fig. 3. Scatterplots between the impervious surface obtained from different methods for the ETM+ image. (a) Reference fractions versus the proposed method, (b) BCI versus the proposed method, and (c) reference fractions versus raw bands.

IV. EXPERIMENTS RESULT AND DISCUSSION

A. ETM+ Image in Guangzhou

1) Fraction Maps: In this paper, we choose high albedo, low albedo, and vegetation as the three fundamental endmembers for the ETM+ image of Guangzhou [54]. Since Guangzhou city is located in a subtropical area with abundant vegetation and without bare soil, it is difficult to use soil as an independent endmember in the medium resolution image. Therefore, in this paper soil is not considered as an endmember for the ETM+ image. We transformed the raw image into 18 new space features in order to properly characterize the spatial information using different scales. Specifically, three attributes were empirically considered: area with reference values λ of 50 and 150, length of diagonal of the bounding box with λ of 30 and 80, and standard deviation with λ of 10 and 20. The obtained

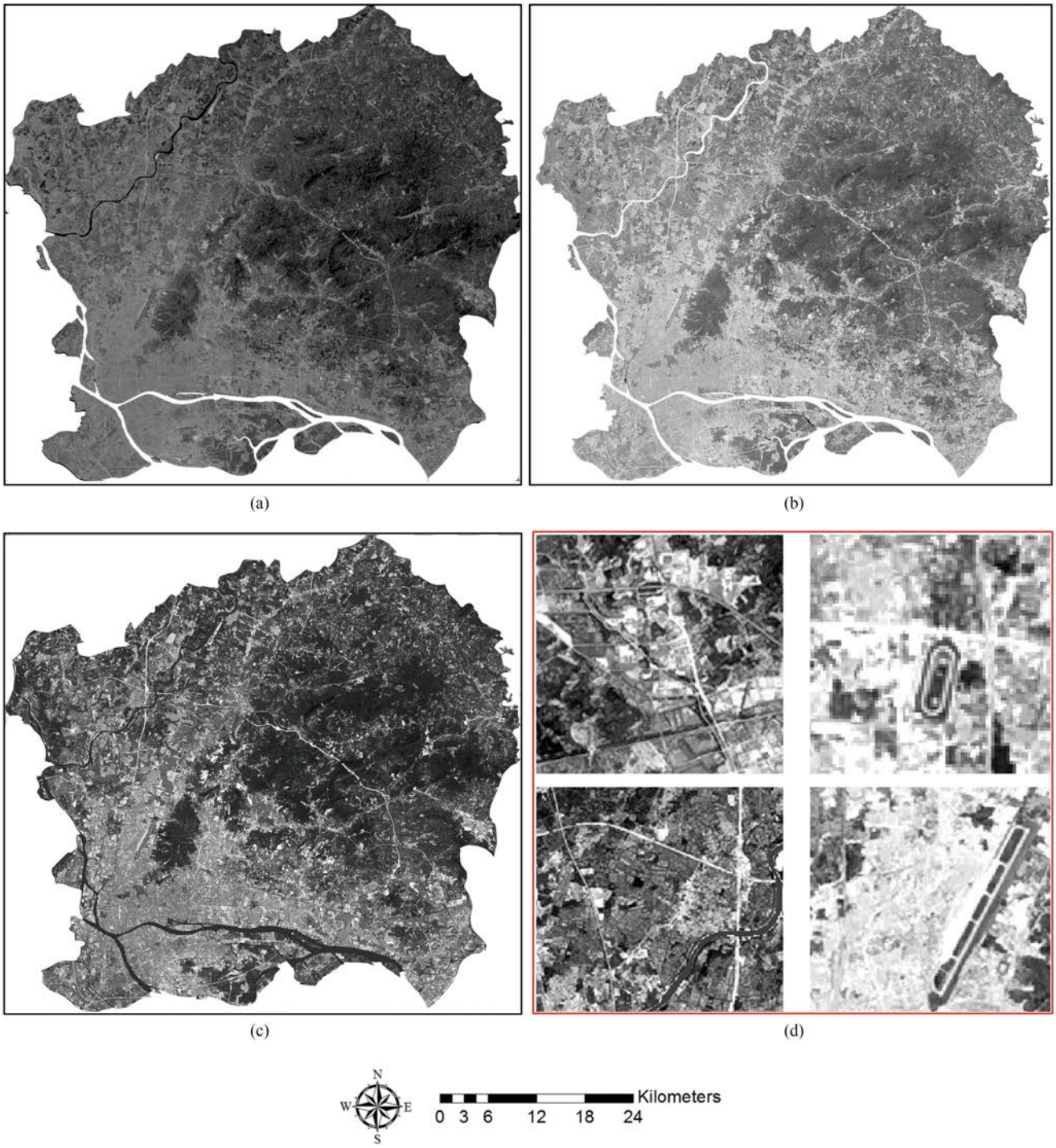

Fig. 4. Impervious surface maps obtained from the ETM+ image by (a) BCI, (b) raw bands, (c) proposed method, and (d) details for observation.

fraction maps are shown in Fig. 2. From Fig. 2, we can observe that the obtained fraction maps exhibit reasonable endmember abundance distributions. One can discriminate the high and low albedo from these three fraction maps. It is worth noting that for the final impervious surface estimation, our results are insensitive with the threshold when they are selected between 40% and 60%. Therefore, the weighted coefficients of f_{low} and f_{high} are empirically set as 0.6 and 0.4, respectively.

2) Accuracy Accessment: To evaluate the accuracy of the impervious surfaces extracted by the proposed method, two types of land covers including *developed areas* and *less developed areas* are considered for verification [1], [10], where the ground reference was derived by manually interpreting randomly selected samples from the Quickbird images. Congalton [61] discussed that for validation a minimum number of 50 samples per land cover is reasonable from both statistical and

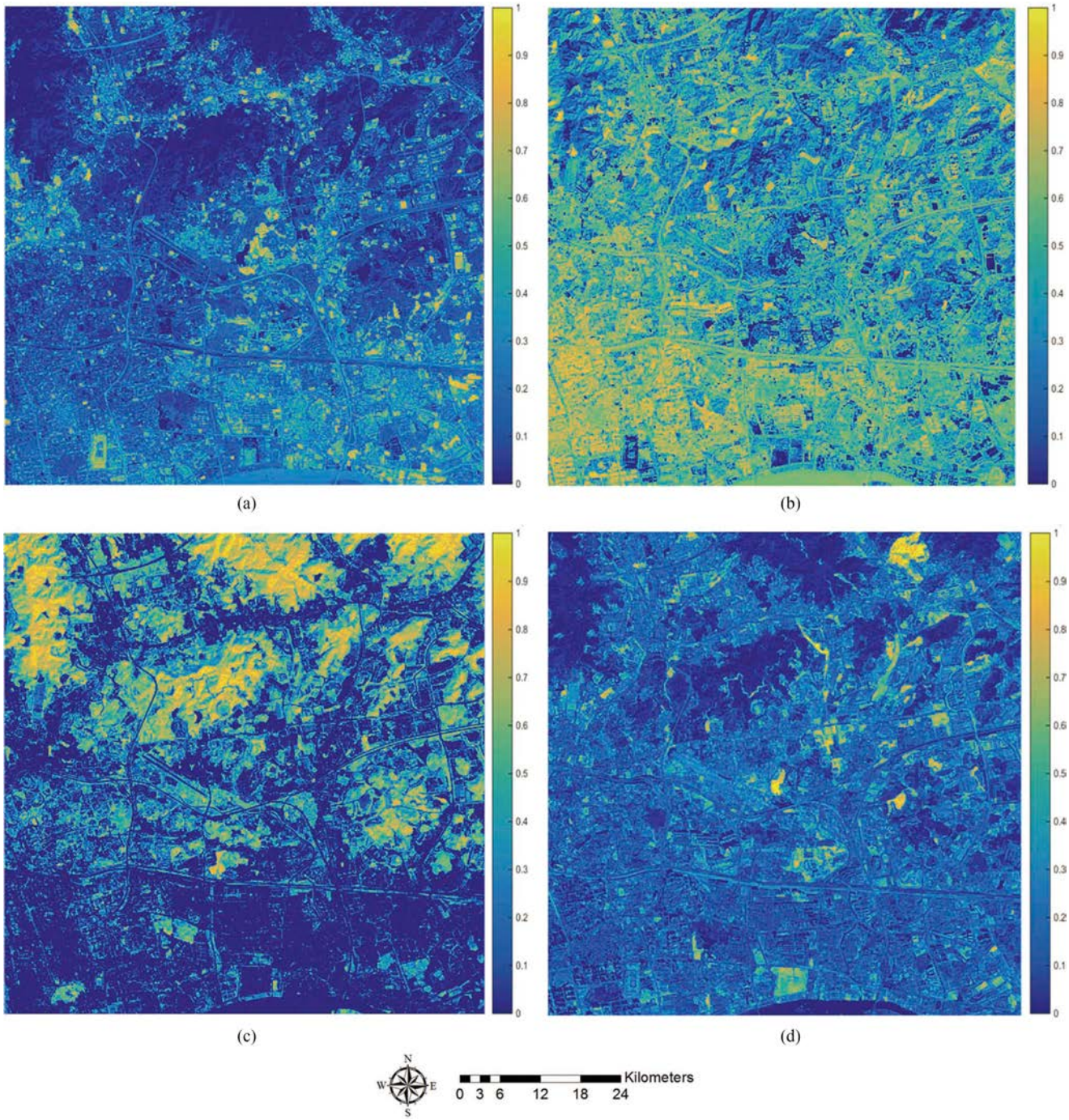

Fig. 5. Three fraction images obtained from the GF-1 image (Guangzhou). (a) High albedo. (b) Low albedo. (c) Vegetation. (d) Bare soil.

practical viewpoints. In this paper, in order to increase the statistical significance, a total number of 300 samples, i.e., 150 samples per land cover, were generated to perform the accuracy assessment. Notice that the reference data covers most of the study area, especially the region with more impervious surfaces. Furthermore, in order to reduce the impact of geometric error between multisource remote sensing images, each sampling unit was designed as a 3×3 pixel block, i.e., a 90×90 m sample size was considered in the ETM+ image [14], [66], [67]. The process of reference interpretation has two main steps. First, the position and the proportion of impervious surface within one sampling unit is figured out. Then, such proportion is considered as a reference for the assessment of the proposed method. Finally, we emphasize that all the samples were interpreted by the same person for the sake of consistency and interpretation quality.

Table I tabulates the results obtained with the three considered error metrics in Guangzhou. In general, the accuracies of the impervious surface estimation are promising and much better than those obtained from the raw bands or the BCI index,

TABLE II
IMPERVIOUS SURFACE ESTIMATION ACCURACY OF THE PROPOSED METHOD (GF-1 IMAGE)

Images	Methods	Areas	RMSE(%)	MAE(%)	Bias(%)
GF-1	Proposed	Developed area (imp$\geq$ 30%)	6.42	9.95	-3.68
		Less developed area (imp$<$ 30%)	7.42	7.42	4.59
		Overall	4.89	6.22	-2.96
	Raw bands [10]	Developed area (imp$\geq$ 30%)	11.57	9.15	-6.52
		Less developed area (imp$<$ 30%)	11.44	8.26	7.52
		Overall	8.36	7.64	5.34

according to the three considered error metrics. Specifically, the overall RMSE is 10.89% and overall MAE is 8.37%. In detail, the estimation of developed areas is more accurate than the estimation of less developed areas. This is expected, since there are higher reflectance areas in well-developed areas, which can be less affected by the pervious land covers. It should also be pointed out that less developed areas are overestimated (with Bias of 8.46%). The reason may be that the low albedo impervious surfaces are highlighted by the proposed method, while some confusion between bare soil or shadows may exist in the ground reference.

The correlation analysis is shown in Fig. 3. It can be observed that both the proposed approach and BCI are linearly correlated with the reference data. The R^2 between the proposed approach and the reference data is 0.7571, 0.06183 higher than that of BCI and the reference data, which is 0.695. It can also be observed that there is a strong linear correlation between imperviousness and Raw bands, with a R^2 of 0.6527.

3) Discussion: In this section, we discuss the performance of the proposed method for the ETM+ images over Guangzhou, comparing with other methods.

The impervious surface maps extracted from the ETM+ image are illustrated in Fig. 4. Generally, impervious surfaces can be classified into two types, i.e., dark impervious surfaces, such as asphalt and pitch, and bright impervious surfaces, such as concrete and cement. It is therefore important to identify the differences between dark impervious surfaces and bright impervious surfaces. As can be observed in Fig. 4(c), in the result obtained by the proposed approach there are clear differences between bright impervious surfaces and dark impervious surfaces, which are however difficult to be identified in the maps obtained by BCI and raw bands. For illustrative purposes, some successful examples are marked and highlighted with red rectangle in Fig. 4(d), highlighting the good performance of the proposed approach. Finally, we can see from Fig. 4(a) and (b) that the region of river is bright. Because the water is not the research region in our topic, we removed this region manually. Therefore, the values of those region are null, and the color is similar to the background.

Moreover, although MAPs can extract the spatial information at some extent, it is difficult to identify the individual objects in medium-resolution images. However, the blocks that cover several streets, forming a square around an area of buildings can obviously be detected, comparing with other methods. Because the high-density residential area generally contains the regular context information, it can be extracted by MAPs. Further, some linear features (e.g., roads in those images) also can be detectable if they have a unique shape [8]. Such details were shown in Fig. 4(d). Because the individual building is hardly detected in the medium-resolution images, the impact of shadow is weak. There is no need to regard the shadow as a unique land cover.

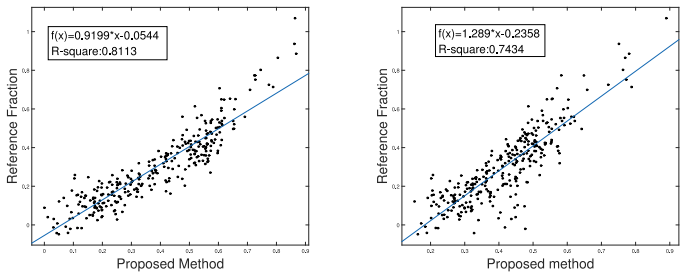

Fig. 6. Scatterplots between different indices and the impervious surface estimated by the proposed method in the GF-1 image. (a) Reference data versus proposed method. (b) Reference data versus the raw bands.

B. GF-1 Image in Guangzhou

1) Fraction Maps: For the GF-1 image, due to its high spatial resolution, we can see that the presence of bare soil is more apparent than in the ETM+ image. Therefore, four endmembers (including high albedo, low albedo, vegetation, and bare soil) are considered for this experiment. The obtained fraction maps are illustrated in Fig. 5. We transformed the raw image into eight new space features in order to properly characterize the spatial information using different scales. Specifically, three attributes were empirically considered: moment of inertia with reference values λ of 0.5 and 0.8, length of diagonal of the bounding box with λ of 20 and 50, and standard deviation with λ of 10 and 20. From Fig. 5, we can observe that the obtained fraction maps also exhibit reasonable distributions. For the final impervious surface estimation, the weighted coefficients of f_{low} and f_{high} are empirically set as 0.4 and 0.6, respectively.

2) Accuracy Accessment: Table II tabulates the results obtained with the three considered error metrics in GF-1 image. It is noted again that there is no BCI experiment for GF-1 image. Similar to the observations with ETM+ image, the accuracies of the impervious surface estimation are promising and much better than those obtained from the raw bands, according to the three considered error metrics. Specifically, the overall RMSE is 4.89%, overall MAE is 6.22%, and the overall Bias is -2.96%.

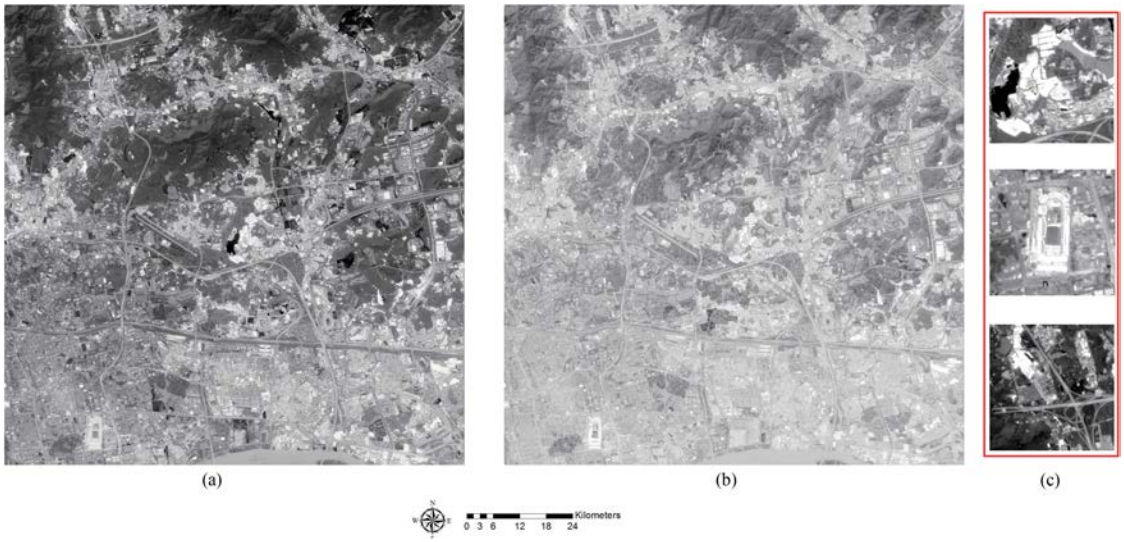

Fig. 7. Fraction images of GF-1. (a) Impervious surface of proposed method. (b) Impervious surface of raw bands. (c) Retails for observation.

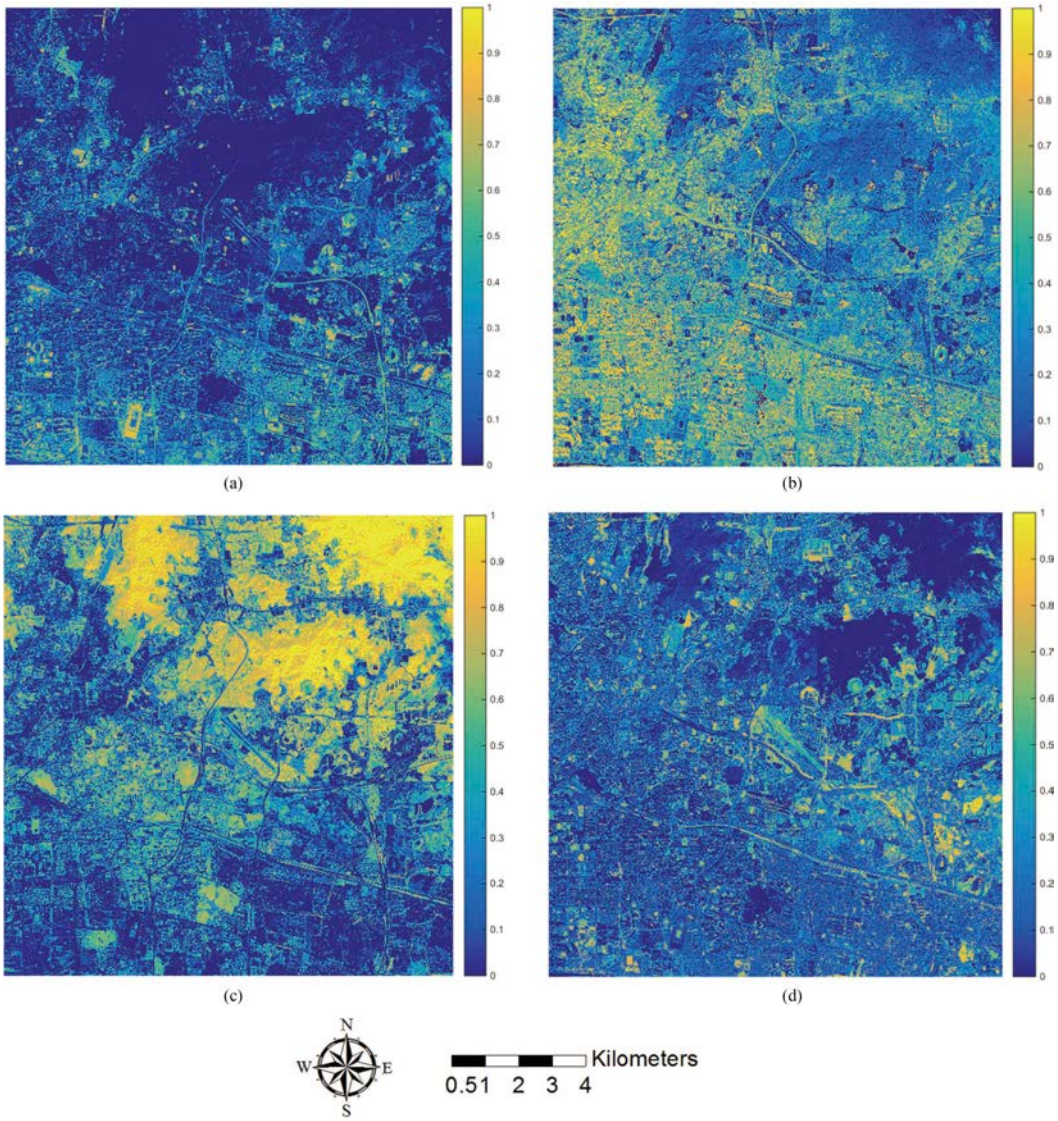

Fig. 8. Four fraction images extracted from the IKONOS image: (a) Low albedo, (b) high albedo, (c) vegetation, and (d) bare soil.

TABLE III
IMPERVIOUS SURFACE ESTIMATION ACCURACY OF THE PROPOSED METHOD (IKONOS IMAGES)

Images	Methods	Areas	RMSE(%)	MAE(%)	Bias(%)
IKONOS	Proposed	Developed area (imp$\geq$ 30%)	4.66	4.91	-1.53
		Less developed area (imp$<$ 30%)	7.81	7.43	4.45
		Overall	7.72	7.67	3.91
	Raw bands [10]	Developed area (imp$\geq$ 30%)	9.47	8.55	-7.58
		Less developed area (imp$<$ 30%)	10.91	10.42	9.47
		Overall	9.92	11.56	7.68
	BCI [63]	Developed area (imp$\geq$ 30%)	12.47	11.68	-6.39
		Less developed area(imp$<$ 30%)	19.01	20.02	9.74
		Overall	12.96	10.86	8.69

The correlation analysis is shown in Fig. 6. It can be observed that the proposed approach are linearly correlated with the reference data. The R^2 between the proposed approach and the reference data is 0.8113, 0.0679 higher than that of raw bands and the reference data, which is 0.7434.

3) Discussion: The impervious surface maps obtained from the GF-1 image are illustrated in Fig. 7. Notice that for the GF-1 image we include the *bare soil* endmember for comparison purposes because it can be regarded as independent endmember in 8-m resolution image. Similar to the observations from the ETM+ results, there is confusion between the bright and dark impervious surfaces. However, as shown in Fig. 7(a), the difference between bright and dark impervious surfaces increases dramatically when the proposed method is used. Compared with the results obtained for the ETM+ image, the proposed method exhibits better performance in the task of discriminating the bright and dark impervious surfaces in the GF-1 image. Moreover, the spatial structures of different land covers are more significant, as the MAPs provide better characterization for extraction purposes. The large concrete/glass constructions, concrete roads, etc., are apparently displayed. Some medium-size objects are well displayed [see Fig. 7(c)], which are hardly detectable in the ETM+ image. This is because the GF-1 image has higher spatial resolution (8 m per pixel) than ETM+ image. Due to the high resolution of GF-1 image, the impact of the shadow of high buildings are more significant than that in ETM+ image. There is little confusion between shadow and low albedo. Therefore, how to alleviate this impact in this framework will be our future work.

C. IKONOS Image in Guangzhou

1) Fraction Maps: For the IKONOS image, due to its high spatial resolution, we can see that the presence of bare soil is more apparent than in the ETM+ image. Therefore, four endmembers (including high albedo, low albedo, vegetation, and bare soil) are considered for this experiment. We transformed the raw image into eight new space features in order to properly characterize the spatial information using different scales. Specifically, three attributes were empirically considered: area with reference values λ of 50 and 150, moment of inertia with λ of 0.2 and 0.5, and standard deviation with λ of 8 and 16. The obtained fraction maps are illustrated in Fig. 8. From Fig. 8, we can observe that the obtained fraction maps also exhibit reasonable distributions. For the final impervious surface estimation, the weighted coefficients of f_{low} and f_{high} are empirically set as 0.5 and 0.5, respectively.

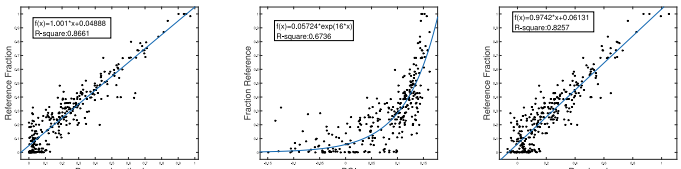

Fig. 9. Scatterplots between different indices and the impervious surface estimated by the proposed method in the IKONOS image. (a) Reference fractions versus the proposed method. (b) Reference fractions versus the BCI. (c) Reference fractions versus raw bands.

2) Accuracy Assessment: Table III tabulates the results obtained with the three considered error metrics in IKONOS image. As the same conclusion with ETM+ and GF-1 image, the accuracies of the impervious surface estimation are promising and much better than those obtained from the raw bands and BCI, according to the three considered error metrics. Specifically, the overall RMSE is 7.72% and overall MAE is 7.67%. And the overall Bias is 3.91%x.

The correlation analysis is shown in Fig. 9. It can be observed that the proposed approach exhibits much better performance than the competitors. Specifically, the proposed approach has a linear correlation with the reference data, while that of BCI is exponential. The R^2 between the proposed approach and the reference data is 0.8661, 0.1925 higher than that of BCI and the reference data, which is 0.6736. Furthermore, this observation is different from the one derived from our experiments with the ETM+ image and GF-1 image, mainly due to the differences in spatial resolution. In the (high spatial resolution) IKONOS image, the pervious surface includes vegetation and bare soil. This is consistent with a visual interpretation of Fig. 10. Here, the correlation between BCI and impervious surface is no longer linear.

3) Discussion: The impervious surface maps obtained from the IKONOS image are illustrated in Fig. 10. Notice that for the IKONOS image we include the *bare soil* endmember for comparison purposes. As shown in Fig. 10(c), the difference

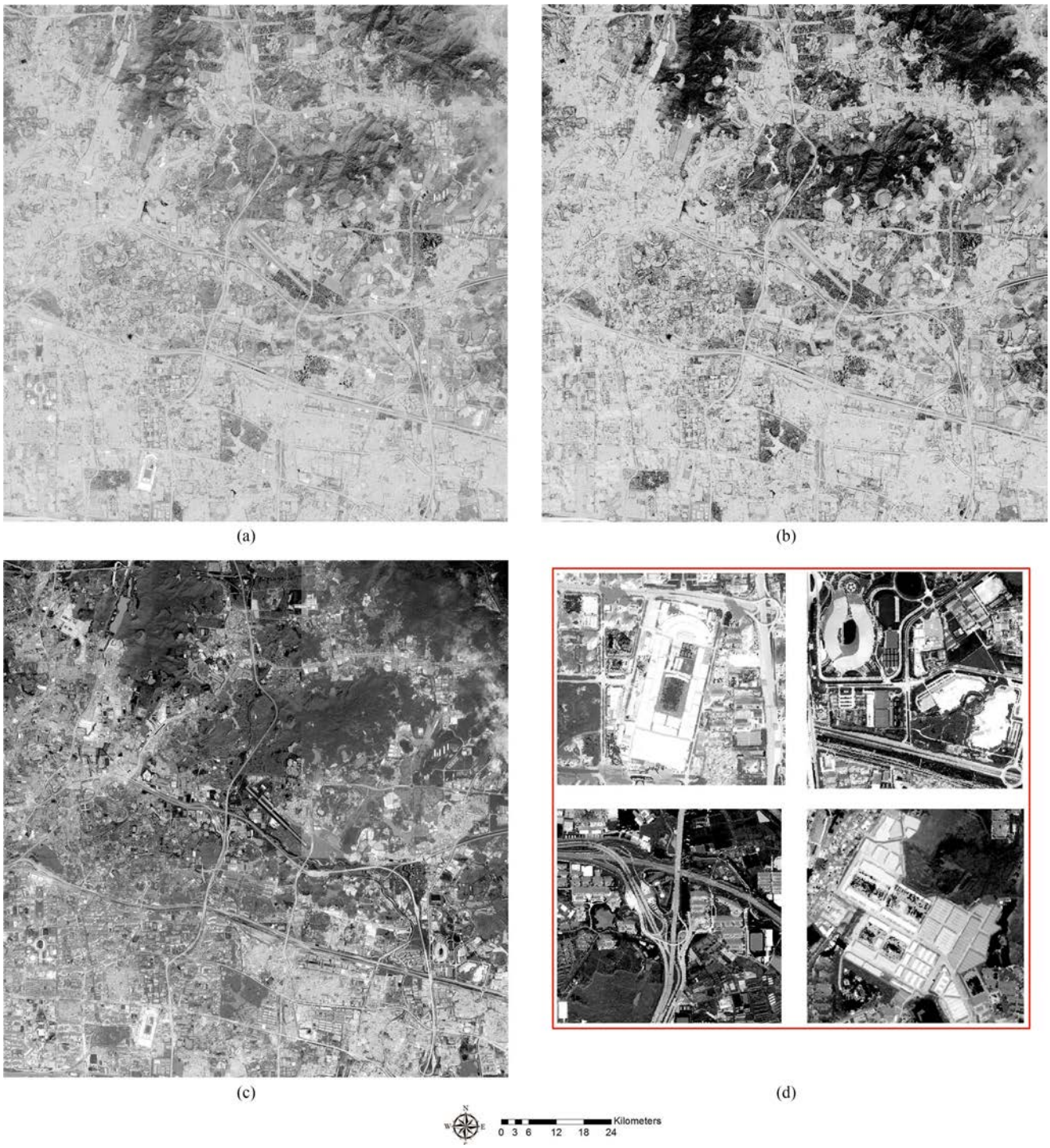

Fig. 10. Fraction images of IKONOS. (a) Raw bands. (b) BCI. (c) Impervious surface of proposed method. (d) Details for observation.

between bright and dark impervious surfaces increases dramatically when the proposed method is used. Compared with the results obtained for the ETM+ and GF-1 image, the proposed method exhibits better performance in the task of discriminating the bright and dark impervious surfaces in the IKONOS image. This is because the IKONOS image has higher spatial resolution (4 m per pixel), and the spatial structures of different land covers are more significant, while the MAPs provide better characterization for extraction purposes. The large concrete/glass constructions, concrete roads, etc. are displayed with bright tones, while asphalt roads, dark building roofs, etc. are displayed as gray tones. In turn, the differences between such land covers are less apparent in the BCI map and raw bands map. Because such methods are lack of process of spatial information extraction. For illustrative purposes, some successful examples are marked and highlighted with red rectangles, highlighting

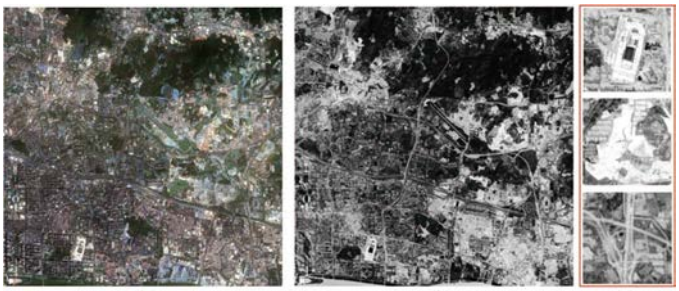

Fig. 11. Fraction images of Sentinel-2. (a) True-color Sentinel-2 image in Guangzhou. (b) Impervious surface of proposed method. (c) Details for observation.

the good performance of the proposed approach. Additionally, the bare soil can be clearly distinguished from the impervious surface, while the other two images exhibit strong confusion for the bare soil class. Similar to the GF-1 case, the impact of shadow are sensitive in 4 m resolution. There is also confusion between shadow and low albedo.

D. Sentinel-2 Image in Guangzhou

For further illustration of the performance of the proposed method in different resolution image, we conduct an additional experiment with Sentinel-2 image. Sentinel-2 images include 12 bands with different spatial resolutions in the range of 10–60 m. In this paper, four bands with resolution 10 m are considered for experiments. The true color map of Sentinel-2 images in Guangzhou and the result of the proposed method are shown in Fig. 11. It can be seen that the impervious surface can be well extracted by the proposed method. Furthermore, the typical buildings can be obviously observed in Fig. 11. Finally, for illustrative purposes, some successful examples are marked and highlighted with red rectangles, highlighting the good performance of the proposed approach [see Fig. 11(c)].

V. Conclusion and Future Lines

Impervious surfaces exhibit unique spatial characteristics in urban environments. The estimation of impervious surfaces is critical for the analysis of urban planning, environmental management, and disaster response. In this paper, we have developed a new method based on morphological attribute profiles for the mapping of impervious surfaces under a SMA model. As one of the most effective method to describe artificial constructions in urban environments, morphological attribute profiles are shown to be effective for the characterization of impervious surfaces, leading to representative spectral signatures for the endmembers in a transformed feature space that integrates spatial and spectral information. Therefore, we can circumvent the heavy computational complexity of multiple endmember analysis (adopted by other methods) as the use of only one signature per endmember, in our context, can lead to robust characterization results.

Four different types of remote sensing data were used to test the new method. Our accuracy assessment shows that the proposed method can achieve very good performance in estimating the impervious surfaces. A comparison with two popular methods, i.e., BCI and the traditional framework of SMA, indicated that the proposed method exhibits good correlation with the ground reference, which is linear in all three remotely sensed images. However, the correlations between BCI with the reference data is exponential IKONOS images. This is because both BCI show some limitations in separating dark impervious surface and soil. This issue can be well tackled by our newly proposed approach. The aforementioned aspects can also be observed from the statistical analysis of the histogram distributions, which reveal a competitive superiority of our newly developed method.

In conclusion, our experiments show that by taking advantage of morphological attribute profiles and SMA, our method can perform precise mapping of impervious surfaces. Although the proposed method achieves good performance in the task of impervious surface estimation, there are also some aspects for improvement. In particular, the existence of bare soil and building shadows may lead to an overestimation of the dark impervious areas by our proposed approach. This aspect deserves future investigation. Therefore, in the future, we will first focus on the problem of discrimination between bright and dark soil in the final impervious surface map. Moreover, since the impact of shadow is significant in the extraction of impervious surface in high resolution images, how to address this problem in our proposed framework will be another target. Furthermore, we will also focus on the study of the weighted coefficients of the high albedo and low albedo, since it is important to make clear the robust and the physical meaning of these thresholds. As a result, our future research will particularly focus on the development of new strategies to mitigate these effects. More state-of-the-art impervious indices, such as combinational build-up index [68], may be for further comparison. Finally, inspired by [69], we will also focus on adapting and implementing the proposed method for large-area mapping of impervious surfaces with more datasets in the future work.

References

[1] M. E. Bauer, N. J. Heinert, J. K. Doyle, and F. Yuan, "Impervious surface mapping and change monitoring using landsat remote sensing," *Proc. ASPRS Annu. Conf.*, 2004, p. 10.

[2] E. T. Slonecker, D. B. Jennings, and D. Garofalo, "Remote sensing of impervious surfaces: A review," *Remote Sens. Rev.*, vol. 20, no. 3, pp. 227–255, Oct. 2001.

[3] D. Lu, Q. Weng, and G. Li, "Residential population estimation using a remote sensing derived impervious surface approach," *Int. J. Remote Sens.*, vol. 102, no. 1, pp. 146–160, Feb. 2006.

[4] Q. Weng, "Modeling urban growth effects on surface runoff with the integration of remote sensing and GIS," *Environ. Manage.*, vol. 28, no. 6, pp. 737–748, Feb. 2001.

[5] A. R. Shahtahmassebi *et al.*, "Remote sensing of impervious surface growth: A framework for quantifying urban expansion and re-densification mechanisms," *Int. J. Appl. Earth Observ. Geoinf.*, vol. 46, pp. 94–112, 2016.

[6] D. Lu and Q. Weng, "Use of impervious surface in urban land-use classification," *Remote Sens. Environ.*, vol. 27, no. 16, pp. 3553–3570, Nov. 2006.

[7] Q. Weng *et al.*, "Land use change analysis in the Zhujiang Delta of China using satellite remote sensing, GIS and stochastic modelling," *J. Environ. Manage.*, vol. 64, no. 3, pp. 273–284, 2002.

[8] Q. Weng, "Remote sensing of impervious surfaces in the urban areas: Requirements, methods, and trends," *Remote Sens. Environ.*, vol. 117, pp. 34–49, Feb. 2012.

[9] M. K. Ridd, "Exploring a VIS(vegetation-impervious surface-soil) model for urban ecosystem analysis through remote sensing: Comparative anatomy for cities," *Int. J. Remote Sens.*, vol. 16, no. 12, pp. 2165–2185, Jan. 1995.

[10] C. Wu and A. T. Murray, "Estimating impervious surface distribution by spectral mixture analysis," *Remote Sens. Environ.*, vol. 84, no. 4, pp. 493–505, Apr. 2003.

[11] D. Lu and Q. Weng, "Spectral mixture analysis of the urban landscape in Indianapolis with Landsat ETM+ imagery," *Photogrammetric Eng. Remote Sens.*, vol. 70, no. 9, pp. 1053–1062, Sep. 2004.

[12] Q. Weng, X. Hu, and H. Liu, "Estimating impervious surfaces using linear spectral mixture analysis with multitemporal ASTER images," *Int. J. Remote Sens.*, vol. 30, no. 18, pp. 4807–4830. May 2009.

[13] G. Sun *et al.*, "Stratified spectral mixture analysis of medium resolution imagery for impervious surface mapping," *Int. J. Appl. Earth Observ. Geoinf.*, vol. 60, pp. 38–48, 2017.

[14] R. L. Powell, D. A. Roberts, P. E. Dennison, and L. L. Hess, "Sub-pixel mapping of urban land cover using multiple endmember spectral mixture analysis: Manaus, Brazil," *Remote Sens. Environ.*, vol. 106, no. 2, pp. 253–267, Sep. 2007.

[15] F. Tang and H. Xu, "Impervious surface information extraction based on hyperspectral remote sensing imagery," *Remote Sens.*, vol. 9, no. 6, p. 550, Oct. 2017.

[16] S. Tompkins, J. F. Mustard, C. M. Pieters, and D. W. Forsyth, "Optimization of endmembers for spectral mixture analysis," *Remote Sens. Environ.*, vol. 59, no. 3, pp. 472–489, Mar. 1997.

[17] C. Song, "Spectral mixture analysis for subpixel vegetation fractions in the urban environment: How to incorporate endmember variability," *Remote Sens. Environ.*, vol. 95, no. 2, pp. 248–263, Jan. 2005.

[18] B. Somers, G. P. Asner, L. Tits, and P. Coppin, "Endmember variability in spectral mixture analysis: A review," *Remote Sens. Environ.*, vol. 115, no. 7, pp. 1603–1616, Sep. 2006.

[19] F. D. Van der Meer and X. Jia, "Collinearity and orthogonality of endmembers in linear spectral unmixing," *Int. J. Appl. Earth Observ. Geoinf.*, vol. 18, pp. 491–503, Oct. 2011.

[20] M. E. Winter, "N-FINDR: An algorithm for fast autonomous spectral endmember determination in hyperspectral data," *SPIE's Int. Sym. Opt. Sci.*, vol. 3753, pp. 266–275, Oct. 1999.

[21] J. C. Harsanyi and C. I. Chang, "Hyperspectral image classification and dimensionality reduction: An orthogonal subspace projection approach," *IEEE Trans. Geosci. Remote Sens.*, vol. 32, no. 4, pp. 779–785, Jul. 1994.

[22] J. M. Nascimento and J. M. Bioucas-Dias, "Vertex component analysis: A fast algorithm to unmix hyperspectral data," *IEEE Trans. Geosci. Remote Sens.*, vol. 43, no. 4, pp. 898–910, Apr. 2005.

[23] X. Lu, H. Wu, Y. Yuan, P. Yan, and X. Li, "Manifold regularized sparse NMF for hyperspectral unmixing," *IEEE Trans. Geosci. Remote Sens.*, vol. 51, no. 5 pp. 2815–2826, May 2013.

[24] J. M. Bioucas-Dias *et al.*, "Hyperspectral unmixing overview: Geometrical, statistical, and sparse regression-based approaches," *IEEE J. Sel. Topics Appl. Earth Observ. Remote Sens.*, vol. 5, no. 2, pp. 354–379, Apr. 2012.

[25] D. A. Roberts and M. Herold, "Imaging spectrometry of urban materials," in *Infrared Spectroscopy in Geochemistry, Exploration Geochemistry, and Remote Sensing* (Short-Course Series, vol. 33), P. King, M. S. Ramsey, and G. Swayze, Eds., London, ON, Canada: Mineral Association Canada, 2004, pp. 155–181.

[26] B. Somers, S. Delalieux, W. W. Verstraeten, and P. Coppin, "A conceptual framework for the simultaneous extraction of sub-pixel spatial extent and spectral characteristics of crops," *Photogrammetric Eng. Remote Sens.*, vol. 75, no. 1, pp. 57–68, Jan. 2009.

[27] W. Li and C. Wu, "A geostatistical temporal mixture analysis approach to address endmember variability for estimating regional impervious surface distributions," *GISci. Remote Sens.*, vol. 53, no. 1, pp. 102–121, Oct. 2016.

[28] F. Fan and Y. Deng, "Enhancing endmember selection in multiple endmember spectral mixture analysis (MESMA) for urban impervious surface area mapping using spectral angle and spectral distance parameters," *Int. J. Appl. Earth Observ. Geoinf.*, vol. 33, pp. 290–301, 2014.

[29] B. Somers, S. Delalieux, W. W. Verstraeten, J. A. N. Van Aardt, G. L. Albrigo, and P. Coppin, "An automated waveband selection technique for optimized hyperspectral mixture analysis," *Int. J. Remote Sens.*, vol. 31, no. 20, pp. 5549–5568, Dec. 2010.

[30] G. P. Asner and D. B. Lobell, "A biogeophysical approach for automated SWIR unmixing of soils and vegetation," *Remote Sens. Environ.*, vol. 74, no. 1, pp. 99–112, Nov. 2000.

[31] J. Zhang, B. Rivard, and A. Sanchez-Azofeifa, "Derivative spectral unmixing of hyperspectral data applied to mixtures of lichen and rock," *IEEE Trans. Geosci. Remote Sens.*, vol. 42, no. 9, pp. 1934–1940, Sep. 2004.

[32] C. I. Chang and B. Ji, "Weighted abundance-constrained linear spectral mixture analysis," *IEEE Trans. Geosci. Remote Sens.*, vol. 44, no. 2, pp. 378–388, Feb. 2006.

[33] B. Somers, S. Delalieux, W. W. Verstraeten, J. Verbesselt, S. Lhermitte, and P. Coppin, "Magnitude-and shape-related feature integration in hyperspectral mixture analysis to monitor weeds in citrus orchards," *IEEE Trans. Geosci. Remote Sens.*, vol. 47, no. 11, pp. 3630–3642, Mar. 2009.

[34] L. He, J. Li, C. Liu, and , S. Li, "Recent advances on spectral-spatial hyperspectral image classification: An overview and new guidelines," *IEEE Trans. Geosci. Remote Sens.*, vol. 56, no. 3, pp. 1579–1597, Mar. 2018.

[35] W. R. Tobler, "A computer movie simulating urban growth in the Detroit region," *Econ. Geography.*, vol. 46, no. 1, pp. 234–240. Oct. 1970.

[36] A. Plaza, P. Martinez, R. Prez, and J. Plaza, "Spatialspectral endmember extraction by multidimensional morphological operations," *IEEE Trans. Geosci. Remote Sens.*, vol. 40, no. 9, pp. 2025–2041, Aug. 2002.

[37] D. Rogge, B. Rivard, J. Zhang, A. Sanchez, J. Harris, and J. Feng, "Integration of spatial–spectral information for the improved extraction of endmembers," *Remote Sens. Environ.*, vol. 110, no. 3, pp. 287–303, Feb. 2002.

[38] C. Deng and C. Wu, "A spatially adaptive spectral mixture analysis for mapping subpixel urban impervious surface distribution," *Remote Sens. Environ.*, vol. 133, no. 1, pp. 62–70, Feb. 2013.

[39] X. Lu, X. Li, and L. Mou, "Semi-supervised multitask learning for scene recognition," *IEEE Trans. Cybern.*, vol. 45, no. 9, pp. 1967–1976, Sep. 2015.

[40] S. Van der Linden and P. Hostert, "The influence of urban structures on impervious surface maps from airborne hyperspectral data," *Remote Sens. Environ.*, vol. 113, no. 11, pp. 2298–2305, Jun. 2004.

[41] M. D. Mura, J. A. Benediktsson, B. Waske, and L. Bruzzone, "Morphological attribute filters for the analysis of very high resolution remote sensing images," *Proc. IEEE Int. Geosci. Remote Sens. Symp.*, 2009, vol. 3, pp. V-84–V-87.

[42] M. D. Mura, J. A. Benediktsson, B. Waske, and L. Bruzzone., "Morphological attribute profiles for the analysis of very high resolution images," *IEEE Trans. Geosci. Remote Sens.*, vol. 48, no. 10, pp. 3747–3762, Nov. 2010.

[43] B. L. Markham and J. L. Barker, "Landsat MSS and TM post-calibration dynamic ranges, exoatmospheric reflectances and at-satellite temperatures," *EOSAT Landsat Technical Notes*, vol. 1, no. 1, pp. 3–8, 1986.

[44] B. Markham and J. Barker, "Thematic Mapper bandpass solar exoatmospheric irradiances," *Int. J. Remote Sens.*, vol. 8, no. 3, pp. 517–523, Dec. 1987.

[45] X. Dai and S. Khorram, "The effects of image misregistration on the accuracy of remotely sensed change detection," *IEEE Trans. Geosci. Remote Sens.*, vol. 36, no. 5, pp. 1566–1577, Sep. 1998.

[46] L. Yangrong, E. Manfred, E. Lynn Usery, and M. Marguerite, "FFT-enhanced IHS transform method for fusing high-resolution satellite images," *ISPRS J. Photogrammetry Remote Sens.*, vol. 61, no. 6, pp. 381–392, Feb. 2007.

[47] K. Sascha and E. Manfred, "Image fusion using the Ehlers spectral characteristics preservation algorithm," *GISci. Remote Sens.*, vol. 44, no. 2, pp. 93–116, Nov. 2007.

[48] M. Pesaresi and J. A. Benediktsson, "A new approach for the morphological segmentation of high-resolution satellite imagery," *IEEE Trans. Geosci. Remote Sens.*, vol. 39, no. 2, pp. 309–320, Jul. 2001.

[49] P. Salembier, A. Oliveras, and L. Garrido, "Antiextensive connected operators for image and sequence processing," *IEEE Trans. Geosci. Remote Sens.*, vol. 7, no. 4, pp. 555–570, Dec. 1998.

[50] J. B. Adams *et al.*, "Classification of multispectral images based on fractions of endmembers: Application to land-cover change in the Brazilian Amazon," *Remote Sens. Environ.*, vol. 52, no. 2, pp. 137–153, Nov. 1995.

[51] D. Roberts, M. Smith, and J. Adams, "Green vegetation, nonphotosynthetic vegetation, and soils in AVIRIS data," *Remote Sens. Environ.*, vol. 44, no. 2/3, pp. 255–269, Jun. 1993.

[52] S. Phinn, M. Stanford, P. Scarth, A. Murray, and P. Shyy, "Monitoring the composition of urban environments based on the vegetation-impervious surface-soil (VIS) model by subpixel analysis techniques," *Int. J. Remote Sens.*, vol. 23, no. 20, pp. 4131–4153, Feb. 2002.

[53] C. Small, "Multitemporal analysis of urban reflectance," *Remote Sens. Environ.*, vol. 81, no. 2, pp. 427–442, May 2002.

[54] C. Small, "Estimation of urban vegetation abundance by spectral mixture analysis," *Int. J. Remote Sens.*, vol. 22, no. 7, pp. 1305–1334, Feb. 2001.
[55] J. Li *et al.*, "Multiple feature learning for hyperspectral image classification," *IEEE Trans. Geosci. Remote Sens.*, vol. 53, no. 3, pp. 1592–1606, Mar. 2015.
[56] J. Settle and N. Drake, "Linear mixing and the estimation of ground cover proportions," *Int. J. Remote Sens.*, vol. 14, no. 6, pp. 1159–1177, Nov. 1993.
[57] F. Van der Meer and S. De Jong, "Improving the results of spectral unmixing of Landsat Thematic Mapper imagery by enhancing the orthogonality of end-members," *IEEE Trans. Geosci. Remote Sens.*, vol. 21, no. 15, pp. 2781–2797, Apr. 2000.
[58] D. C. Heinz, "Fully constrained least squares linear spectral mixture analysis method for material quantification in hyperspectral imagery," *Remote Sens. Environ.*, vol. 39, no. 3, pp. 529–545, May 2001.
[59] S. K. Mcfeeters, "The use of the Normalized Difference Water Index (NDWI) in the delineation of open water features," *Int. J. Remote Sens.* vol. 17, no. 7, pp. 1425–1432, Oct. 1996.
[60] J. Yang and P. Li, "Impervious surface extraction in urban areas from high spatial resolution imagery using linear spectral unmixing," *Remote Sens. Environ.*, vol. 1, pp. 61–71, Jul. 2015.
[61] R. G. Congalton, "A review of assessing the accuracy of classifications of remotely sensed data," *Remote Sens. Environ.*, vol. 37, no. 1, pp. 35–46, Feb. 1991.
[62] A. A. Green, M. D. Craig, and S. Cheng, "The application of the minimum noise fraction transform to the compression and cleaning of hyper-spectral remote sensing data," *Proc. Int. Geosci. Remote Sens. Symp., Remote Sens., Moving Toward 21st Century*, 1988, pp. 550–565.
[63] C. Deng and C. Wu, "BCI: A biophysical composition index for remote sensing of urban environments," *Remote Sens. Environ.*, vol. 127, no. 1, pp. 247–259, Feb. 2012.
[64] C. Huang, B. Wylie, L. Yang, C. Homer, and G. Zylstra, "Derivation of a tasselled cap transformation based on Landsat 7 at-satellite reflectance," *Int. J. Remote Sens.*, vol. 27, no. 8, pp. 1741–1748, Sep. 2002.
[65] J. H. Horne, "A tasseled cap transformation for IKONOS images," *Proc. ASPRS Annu. Conf.*, 2003, p. 9.
[66] D. A. Roberts, D. A. Quattrochi, G. C. Hulley, S. J. Hook, and R. O. Green, "Synergies between VSWIR and TIR data for the urban environment: An evaluation of the potential for the Hyperspectral Infrared Imager (HyspIRI) Decadal Survey mission," *Remote Sens. Environ.*, vol. 117, pp. 83–101, Jul. 2012.
[67] S. V. Stehman and R. L. Czaplewski, "Design and analysis for thematic map accuracy assessment: Fundamental principles," *Remote Sens. Environ.*, vol. 64, no. 3, pp. 331–344, Jun. 1998.
[68] G. Sun, X. Chen, X. Jia, Y. Yao, and Z. Wang, "Combinational build-up index (CBI) for effective impervious surface mapping in urban areas," *IEEE J. Sel. Topics Appl. Earth Observ. Remote Sens.*, vol. 9, no. 5, pp. 2081–2092, May 2016.
[69] L. Yang, Ch. Huang, C. G. Homer, B. K. Wylie, and M. J. Coan, "An approach for mapping large-area impervious surfaces: Synergistic use of Landsat-7 ETM+ and high spatial resolution imagery," *Can. J. Remote Sens.*, vol. 29, no. 2, pp. 230–240, Jun. 2003.

Changyu Zhu received the B.S. degree from the University of Science and Technology Liaoning, Anshan, China, in 2014, and the M.E. degree from the Sun Yat-sen University, Guangzhou, China, in 2018, both in remote sensing.

His research interests include the application of remote sensing and urban environment analysis.

Jun Li (M'13–SM'16) received the B.S. degree in geographic information systems from Hunan Normal University, Changsha, China, in 2004, the M.E. degree in remote sensing from Peking University, Beijing, China, in 2007, and the Ph.D. degree in electrical engineering from the Instituto de Telecomunicações, Instituto Superior Tcnico (IST), Universidade Tcnica de Lisboa, Lisbon, Portugal, in 2011.

From 2007 to 2011, she was a Marie Curie Research Fellow with the Departamento de Engenharia Electrotcnica e de Computadores and the Instituto de Telecomunicações, IST, Universidade Tcnica de Lisboa, in the framework of the European Doctorate for Signal Processing (SIGNAL). She has also been actively involved in the Hyperspectral Imaging Network, a Marie Curie Research Training Network involving 15 partners in 12 countries, intended to foster research, training, and cooperation on hyperspectral imaging at the European level. Since 2011, she has been a Postdoctoral Researcher with the Hyperspectral Computing Laboratory, Department of Technology of Computers and Communications, Escuela Politcnica, University of Extremadura, Cceres, Spain. From 2014 to 2018, she was a Professor with Sun Yat-sen University, Guangzhou, China. She is currently a Professor with Hunan University, Changsha, China. Her research interests include hyperspectral image classification and segmentation, spectral unmixing, signal processing, and remote sensing.

Dr. Li is an Associate Editor for the IEEE JOURNAL OF SELECTED TOPICS IN APPLIED EARTH OBSERVATIONS AND REMOTE SENSING. She has been a Reviewer for several journals, including the IEEE TRANSACTIONS ON GEOSCIENCE AND REMOTE SENSING, the IEEE GEOSCIENCE AND REMOTE SENSING LETTERS, *Pattern Recognition*, *Optical Engineering*, the *Journal of Applied Remote Sensing*, and *Inverse Problems and Imaging*.

Shaoquan Zhang received the B.S. and M.E. degrees from the Nanchang Institute of Technology, Nanchang, China, in 2012 and 2015, respectively, and the Ph.D. degree from the Sun Yat-sen University, Guangzhou, China, in 2018, all in remote sensing.

He is currently a Lecturer with the Jiangxi Province Key Laboratory of Water Information Cooperative Sensing and Intelligent Processing, Nanchang Institute of Technology, Nanchang, China. His research interests include hyperspectral unmixing, sparse representation, and machine learning.

Changshan Wu received the B.S. degree in geography from Peking University, Beijing, China, in 1995, the M.S. degree in remote sensing from the Institute of Remote Sensing Applications, Chinese Academy of Sciences, Beijing, China, in 1999, and the Ph.D. degree in geography from The Ohio State University, Columbus, OH, USA, in 2003.

Since 2003, he has been with the Department of Geography, University of Wisconsin-Milwaukee, where he is currently a Full Professor. He is the author of more than 80 journal articles and book chapters. His research interests include remote sensing and urban analysis, and geographic information science.

Dr. Wu was the recipient of the University Consortium Geographic Information Science Intergraph Young Scholar Award in 2006.

Bing Zhang (M'11–SM'12) received the B.S. degree in geography from Peking University, Beijing, China, in 1991, and the M.S. and Ph.D. degrees in remote sensing from the Institute of Remote Sensing Applications, Chinese Academy of Sciences, Beijing, China, in 1994 and 2003, respectively.

He is currently a Full Professor and the Deputy Director of the Institute of Remote Sensing and Digital Earth, Chinese Academy of Sciences (CAS), where he has been leading key scientific projects in the area of hyperspectral remote sensing for more than 20 years. He has developed five software systems in the image processing and applications. He has authored more than 300 publications, including more than 170 journal papers. He has edited six books/contributed book chapters on hyperspectral image processing and subsequent applications. His research interests include the development of mathematical and physical models and image processing software for the analysis of hyperspectral remote sensing data in many different areas.

His creative achievements were rewarded ten important prizes from the Chinese Government, and special government allowances of the Chinese State Council. He was awarded the National Science Foundation for Distinguished Young Scholars of China in 2013, and was awarded the 2016 Outstanding Science and Technology Achievement Prize of the Chinese Academy of Sciences, the highest level of Awards for the CAS scholars. He is currently an Associate Editor for the IEEE JOURNAL OF SELECTED TOPICS IN APPLIED EARTH OBSERVATIONS AND REMOTE SENSING and the IEEE GEOSCIENCE AND REMOTE SENSING LETTERS. He has been a Technical Committee Member of the IEEE Workshop on Hyperspectral Image and Signal Processing since 2011, and the President of the Hyperspectral Remote Sensing Committee of China National Committee of International Society for Digital Earth since 2012. He was a Student Paper Competition Committee member in IGARSS 2015, 2016, and 2017.

Lianru Gao (M'11–SM'18) received the B.S. degree in civil engineering from Tsinghua University, Beijing, China, in 2002, and the Ph.D. degree in cartography and geographic information system from Institute of Remote Sensing Applications, Chinese Academy of Sciences (CAS), Beijing, China, in 2007.

He has been a visiting scholar with the University of Extremadura, Cceres, Spain, in 2014, and with the Mississippi State University, Starkville, MS, USA, in 2017. He is currently a Professor with the Key Laboratory of Digital Earth Science, Institute of Remote Sensing and Digital Earth, CAS. In the last ten years, he has been the project investigator (PI) of ten scientific research projects at national and ministerial levels, including projects by the National Natural Science Foundation of China (2010–2012, 2016–2019, 2018–2020), and by the Key Research Program of the CAS (2013–2015), etc. He has published more than 120 peer-reviewed papers, and there are 50 journal papers included by Science Citation Index. He was a coauthor of an academic book entitled *Hyperspectral Image Classification and Target Detection*. He obtained 17 National Invention Patents and 4 Software Copyright Registrations in China. His research interests include models and algorithms for hyperspectral image processing, analysis, and applications.

Dr. Gao was awarded the Outstanding Science and Technology Achievement Prize of the CAS in 2016, and the China National Science Fund for Excellent Young Scholars in 2017. He received the recognition of the Best Reviewers of the IEEE JOURNAL OF SELECTED TOPICS IN APPLIED EARTH OBSERVATIONS AND REMOTE SENSING in 2015, and the Best Reviewers of the IEEE TRANSACTIONS ON GEOSCIENCE AND REMOTE SENSING in 2017.

Antonio Plaza (M'05–SM'07–F'15) was born in Caceres, Spain, in 1975. He is currently an Associate Professor (with accreditation for Full Professor) with the Department of Technology of Computers and Communications, University of Extremadura, Badajoz, Spain, where he is the Head of the Hyperspectral Computing Laboratory, one of the most productive research groups working on remotely sensed hyperspectral data processing worldwide. He has been the advisor of 12 Ph.D. dissertations and more than 30 M.Sc. theses. He was the Coordinator of the Hyperspectral Imaging Network, a European project with total funding of 2.8 million Euro. He has authored more than 500 publications, including 152 journal papers (more than 100 in IEEE journals), 22 book chapters, and more than 240 peer-reviewed conference proceeding papers (94 in IEEE conferences). He has reviewed more than 500 manuscripts for more than 50 different journals. He has edited a book on *High-Performance Computing in Remote Sensing* (CRC Press, 2007) and guest edited 9 special issues on hyperspectral remote sensing for different journals. His research interests include hyperspectral data processing and parallel computing of remote sensing data.

Dr. Plaza is a Fellow of IEEE "for contributions to hyperspectral data processing and parallel computing of Earth observation data." He is also an Associate Editor for IEEE ACCESS, and was a member on the Editorial Board of the IEEE GEOSCIENCE AND REMOTE SENSING NEWSLETTER during 2011–2012 and the IEEE GEOSCIENCE AND REMOTE SENSING MAGAZINE in 2013. He was also a member of the steering committee of the IEEE JOURNAL OF SELECTED TOPICS IN APPLIED EARTH OBSERVATIONS AND REMOTE SENSING (JSTARS). He is a recipient of the recognition of Best Reviewers for the IEEE GEOSCIENCE AND REMOTE SENSING LETTERS in 2009, and for the IEEE TRANSACTIONS ON GEOSCIENCE AND REMOTE SENSING in 2010—a journal for which he served as Associate Editor from 2007 to 2012; the 2013 Best Paper Award of the JSTARS journal; the most highly cited paper during 2005–2010 in the *Journal of Parallel and Distributed Computing*; the Best Paper Awards at the IEEE International Conference on Space Technology and the IEEE Symposium on Signal Processing and Information Technology; and the Best Ph.D. Dissertation award at the University of Extremadura—a recognition also received by six of his Ph.D. students. He served as the Director of education activities for the IEEE Geoscience and Remote Sensing Society (GRSS) during 2011–2012, and has been the President of the Spanish Chapter of IEEE GRSS since November 2012. He was a Proposal Evaluator for the European Commission, the National Science Foundation, the European Space Agency, the Belgium Science Policy, the Israel Science Foundation, and the Spanish Ministry of Science and Innovation. He is currently the Editor-in-Chief for the IEEE TRANSACTIONS ON GEOSCIENCE AND REMOTE SENSING journal. For more details visit http://www.umbc.edu/rssipl/people/aplaza.